NJC

PAPER

View Article Online
View Journal | View Issue



Cite this: *New J. Chem.*, 2018, **42**, 555

# Facile preparation and investigation of the properties of single molecular POSS-based white-light-emitting hybrid materials using click chemistry†

Gang Zhao,[a] Yakun Zhu,[a] Shanyi Guang,*[b] Fuyou Ke[a] and Hongyao Xu *[a]

Received 26th September 2017,
Accepted 22nd November 2017

DOI: 10.1039/c7nj03692b

rsc.li/njc

Recently, organic white light emitting devices (OWLEDs) have attracted great interest in flexible displays and solid state lighting devices. Here we report a kind of novel POSS-based white-light-emitting single molecular nanohybrid (POSS-WLED), which was precisely and controllably prepared *via* click chemistry by simply controlling the feed ratio of blue (**B**) and yellow (**Y**) emitting units. It was found that the self-absorption of the emitting component and the intramolecular energy transfer were well adjusted based on theoretical simulations and molecular design. The incorporation of nanosized inorganic POSS effectively restrained intramolecular rotation (RIR) and shows a significant decoupling effect of the emitter and an AIE (aggregation induced enhancement) effect, which provided an important contribution to the high emission efficiency of hybrid molecules. The resultant nanometer organic–inorganic hybrid ($\mathbf{W_{62}}$) exhibited a significantly enhanced emission in the solid film ($\Phi_{film}$ = 95%) because of the significant AIE effect which is attributed to the incorporation of nano-sized POSS moieties. Herein, this work will provide a novel strategy for the design and preparation of highly efficient white-light-emitting molecules with a high emission efficiency, thermal stability, and good film forming ability.



## 1. Introduction

Nowadays, single molecular organic white light emitting materials, as novel type of luminescent media, have become increasingly popular in contemporary research owing to their potential for applications in flexible displays and solid state lighting sources.[1–8] Compared with multicomponent molecular emitters of white-light-emitting devices (WLEDs), single molecular organic white light emitters have exhibited some prominent advantages such as perfect color reproducibility and stability.[9–17] In the previous literature, white-light-emitting single molecules are mainly based on polymers, which are composed of covalently linked different emitter components on the backbone or in side groups. The white light emissions in these polymers are generated *via* utilizing partial energy transfer from a wider band-gap donor component to a narrower band-gap acceptor.[18–22,43] However, the inherent poor purity, low multi-polydispersity, and low thermal properties of polymers have greatly limited their luminous efficiency and practical applications. Hence, design and preparation of organic white-light-emitting macromolecules with high thermal properties and good luminous efficiency will be a key issue for their application in flexible displays. However, the inevitable energy transfer makes the molecular design difficult. To the best of our knowledge, only Park and his coworkers[23,24] reported an excited-state intramolecular proton transfer molecule composed of covalently linked blue- and orange-light-emitting moieties, whose energy transfer was entirely frustrated and white luminescence was achieved. However, small organic molecules often exhibited low thermal properties.

Accordingly, it is a challenge to seek an alternate material system that combines the benefits of organic small molecules (*e.g.*, high purity), inorganic moieties (high thermal stability) and polymers (*e.g.*, good film forming ability and low processing cost). The discovery of polyhedral oligomeric silsesquioxanes (POSSs) with a special structure provided an important tool to solve these problems. POSSs are nanometer-sized cube-like molecules with an inorganic core surrounded by eight organic corner groups (active or inert), which have been demonstrated to be an excellent platform and building block for fabricating novel 3D organic–inorganic molecular hybrid materials with a number of desirable properties.[25–31] A rigid POSS cage enables significantly improving the thermal and mechanical properties of the materials. In our previous work, many POSSs containing

[a] *State Key Laboratory for Modification of Chemical Fibers and Polymer Materials & College of Material Science and Engineering, Donghua University, Shanghai 201620, China. E-mail: hongyaoxu@163.com; Tel: +86-21-67792874*
[b] *School of Chemistry, Chemical and Bioengineering, Donghua University, Shanghai, 201620, China*

† Electronic supplementary information (ESI) available. See DOI: 10.1039/c7nj03692b

organic–inorganic molecular hybrids were designed and prepared for the investigation of preparation methods of these hybrids and enhancement mechanisms of their thermal properties.[29–33] Moreover, some functional hybrids with high thermal stability and nonlinear optical properties were prepared and the enhancement mechanisms of their optical properties were investigated.[34,41,42] It was found that a suitable molecular design will effectively improve the thermal stability and optical properties.

In this paper, based on theoretical simulations, three POSS-based luminous single molecular nanohybrids containing a yellow monochromatic emitter (**Y**) with a large Stokes shift and a blue monochromatic emitter (**B**) were designed and prepared, where both emitters possess similar absorption spectra to avoid the strong self-absorption between different emitters. The partial energy transfer from **B** to **Y** is allowed for effectively adjusting the balance of the white light emission. It is hopefully realized that the incorporation of nanosized inorganic POSSs can inhibit molecular aggregation and improve the luminous efficiency. In addition, the emission mechanism of white light of single nanohybrid molecules was also investigated in detail on the basis of experimental and theoretical methods.

## 2. Experimental

### 2.1. Materials

Unless otherwise noted, all commercial reagents were used as received. $PdCl_2(PPh_3)_2$, 9-bromoanthracene, 1,2-dimethoxyethane- and ethynyltrimethylsilane were purchased from J&K Scientific Ltd. $NaN_3$, 4-bromobenzaldehyde and CuI were purchased from Shanghai Jiachen Chemical Plant. Acetylacetone, NaOH, tetrabutylammonium bromide, DMSO, 1,4-dioxane, KF, CuBr, $PPh_3$ and THF were purchased from Shanghai Chemical Reagent Company. Octakis(azidomethyl)(dimethylsiloxy)octasilsequioxane (ODZMS) was obtained according to the literature procedure.[35] The TEA and THF solutions were distilled immediately prior to use.

### 2.2. Instruments

FTIR spectra were recorded using a KBr disk and a Nicolet NEXUS 8700 FTIR spectrometer. $^1$H NMR spectra were collected on a Bruker DMX-400 spectrometer using chloroform ($CDCl_3$) as a solvent. $^{29}$Si NMR measurements were obtained at room temperature using a Bruker DMX-400 spectrometer at a resonance frequency of 79.49 MHz. Matrix assisted laser desorption ionization time of flight mass spectrometry (MALDI-TOF MS) was carried out using a Voyager-DE RP in linear and reflection modes. The optical properties of the samples were measured using a Shimadzu UV-265 spectrophotometer and a FP6600 Fluorescence spectrometer with a 1 cm quartz cell in tetrahydrofuran (THF, $1 \times 10^{-5}$ M). Elemental analysis (EA) was carried out using a CHNOS Elemental Analyzer, vario EI III. DSC (differential scanning calorimetry) was performed on a TA instruments DSC 9000 equipped with a liquid nitrogen cooling accessory unit under a continuous purge (50 mL min$^{-1}$). The scan process was carried out at a heating rate of 10 °C min$^{-1}$ within the temperature range 20–300 °C. Thermogravimetric analysis (TGA) was performed using a Perkin-Elmer TGA under a nitrogen atmosphere at a heating rate of 10 °C min$^{-1}$. The atomic force microscopy (AFM) images of films were obtained in the trapping mode on an Agilent 5500 AFM.

**Quantum efficiency.** Photoluminescence excitation (PLE) was defined through a modification of the relative approach to describe *via* Crosby and Demas using 1,10-diphenylanthracence as a reference. The absorption at 365 nm was established for each materials at different concentrations (maximum absorption of 20%). Then these samples were diluted equally so as to prevent excimer formation and fluorimeter saturation, and the whole area of the emission spectrum was calculated. For each solvent, absorption and emission measurements were duplicated at least two times and averaged. The slope of a plot of emission *versus* absorption was ascertained for each material, and according to the equation $\Phi_{PL(x)} = (A_s/A_x)(F_x/F_s)(n_x/n_s)^2\Phi_{PL(x)}$ the relative quantum efficiency was calculated.

Where x is the sample to be evaluated, s is the reference, $A$ is the absorption at the excitation wavelength, $F$ is the entire integrated emission, $n$ is the refraction index of the solvent, and $\Phi_{PL}$ is the quantum yield. The materials of PLQE ($\Phi$) in film were collected using 9,10-diphenylanthrancene (scattered in the PMMA film with a concentration lower than $1 \times 10^{-3}$ M and a PLQE of 83%) as a standard.

### 2.3. Synthesis

The synthesis of the monomers and hybrid materials is shown in Schemes 1 and 2, respectively. The experimental details are described as follows:

**2.3.1. Synthesis of 2-methyl-6-*tert*-butyl-4*H*-pyrone (2).** The compound **2** was obtained according to the literature procedure.[36] The isolated yield of the product was 80%. $^1$H NMR (400 MHz, 298 K, $CDCl_3$): $\delta$ = 6.16 (s, 1H, $J$ = 2.17 Hz, Pr–H), 6.07 (s, 1H, Pr–H), 2.43 (s, 3H, $CH_3$), 1.35 (s, 9H, $C(CH_3)_3$). FTIR (KBr), $\nu$ (cm$^{-1}$): 3070 (w, C═C–H), 2972, 2932, 2871 (m, –CH), 1655 (s, C═O).

**2.3.2. Synthesis of 2-(2-*tert*-butyl-6-methyl-4*H*-4-pyranyl) malononitrile (3).** The compound **3** was prepared by the reaction compound **2** and malononitrile according to the literature procedure.[36] $^1$H NMR (400 MHz, 298 K, $CDCl_3$): $\delta$ = 6.49–6.50 (m, 2H, Pr–H), 2.27 (s, 3H, $CH_3$), 1.23 (s, 9H, $C(CH_3)_3$). FTIR (KBr), $\nu$ (cm$^{-1}$): 2970, 2879 (m, –$CH_3$), 2212 (s, –CN), 1652 (C═C), 1342, 1275, 1201 (m, C–O–C).

**2.3.3. Synthesis of 4-trimethylsilyl ethynylbenzaldehyde (4).** The compound **3** was also prepared based on the previously reported literature.[37] Yield: 85%. $^1$H NMR (400 MHz, 298 K, $CDCl_3$): $\delta$ = 9.93 (s, 1H, CHO), 7.74–7.76 (d, 2H, $J$ = 8.3 Hz, Ar-H), 7.52–7.55 (d, 2H, $J$ = 8.3 Hz, Ar-H), 0.20 (s, 9H, $CH_3$). FTIR (KBr), $\nu$ (cm$^{-1}$): 2961 (Si–CH), 2830, 2732 (HC═O), 2159 (C≡C), 1705 (C═C), 1251, 845 (Si–C).

**2.3.4. Synthesis of 4-ethynylbenzaldehyde (5).** Compound **5** was synthesized using a modified literature procedure.[38] Yield 80%. $^1$H NMR (400 MHz, 298 K, $CDCl_3$): $\delta$ = 9.95 (s, 1H, $H^4$), 7.77–7.79 (d, 2H, $J$ = 8.2Hz, $H^4$), 7.56–7.58 (d, 2H, $J$ = 8.2 Hz, $H^3$), 3.23 (s, 1H, $H^1$). FTIR (KBr, cm$^{-1}$): 3293 (s, C≡CH), 2107 (C≡C), 1666 (HC═O).

 

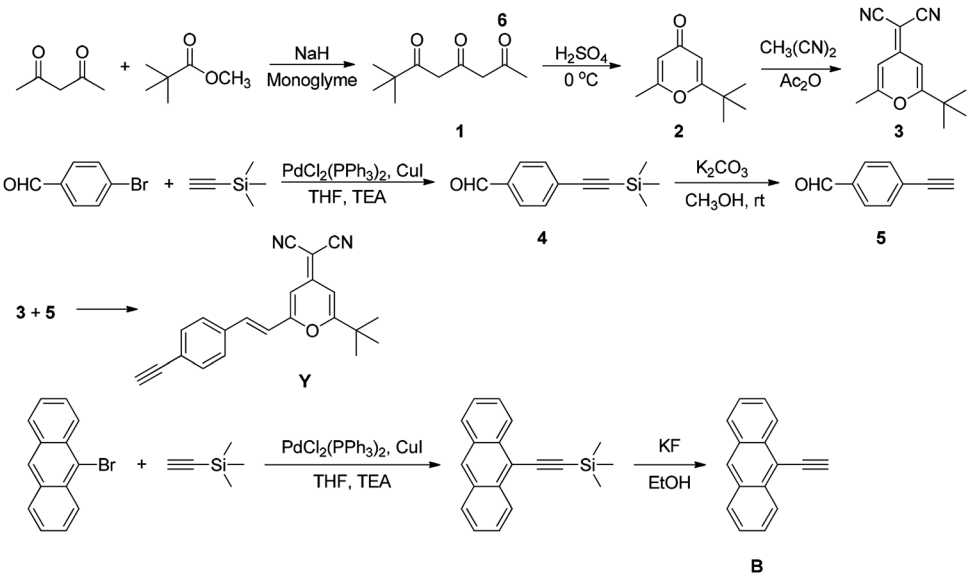


Scheme 1 The synthetic route of the blue monomer (**B**) and the yellow monomer (**Y**).

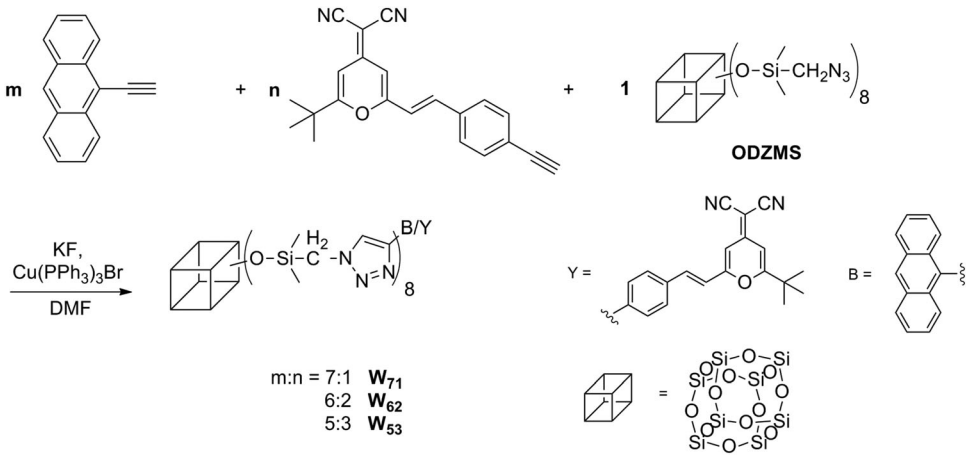


Scheme 2 The synthetic route of white-light hybrids.

**2.3.5. Synthesis of 2-(2-*tert*-butyl-6-(4-alkynyl styrene)-4*H*-4-sub pyranyl) two propylene nitrile (Y).** **3** (1.07 g, 5 mmol), **5** (0.68 g 5.2 mmol) and 0.2 mL pyridine were dissolved in 50 mL anhydrous acetonitrile and refluxed for 24 h. After cooling to room temperature, **Y** of the resultant precipitate was filtered and rinsed with enough acetonitrile. The crude was recrystallized using the mixture solution of THF and ethanol to give yellow crystal **Y** in 70% yield. $^1$H NMR (400 MHz, 298 K, $CDCl_3$): $\delta$ = 7.43–7.49 (m, 5H, $H^{2-6}$), 7.28–7.32 (d, 1H, $H^7$), 6.64–6.64 (m, 2H, $H^{8,9}$), 3.23 (s, 1H, $H^1$), 1.31 (s, 1H, $H^{10}$). FTIR (KBr), $\nu$ ($cm^{-1}$): 3243 (s, C≡CH), 2970, 2926, 2855 (w, $CH_3$), 2103 (C≡C), 1650 (HC═O), 1508 (C═C). $^{13}$C NMR (100 MHz, 298 K, $CDCl_3$): $\delta$ =32.54, 35.51, 70.12, 81.43, 42.38, 90.83, 112.54, 115.58, 116.63, 121.97, 127.74, 132.26, 134.41, 164.57, 178.43. MALDI-TOF MS $[C_{22}H_{18}N_2O + 2H]^+$: calcd $(M + 2H)^+/z$, 326.1403; found $m/z$, 326.1675.

**2.3.6. Synthesis of 9-trimethylsilylacetylene anthracene (6).** Compound **6** was prepared in analogy to a literature procedure.[39] Yield 85%. $^1$H NMR (400 MHz, 298 K, $CDCl_3$): $\delta$ = 8.94–9.01 (m, 3H, $H^{1,5}$), 8.51–8.53 (d, 2H, $J$ = 8.3 Hz, $H^2$), 8.00–8.14 (m, 4H, $H^{3,4}$), 0.20 (s, 9H, $H^6$). FTIR (KBr), $\nu$ ($cm^{-1}$): 3047 (m, Ar-H), 2956 (m; $-CH_3$), 2144 (w, C≡C), 1623, 884 (m, Ar), 1259, 843, 728 (s, Si $(CH_3)_3$).

**2.3.7. Synthesis of 9-ethynyl anthracene (B).** Compound **B** was obtained using a modified literature procedure.[39] Yield 78%. $^1$H NMR (400 MHz, 298 K, $CDCl_3$): $\delta$ = 8.44–8.59 (m, 4H, $H^{2,5}$), 7.99–8.03 (m, 1H, $H^6$), 7.46–7.63 (m, 4H, $H^{3,4}$), 3.99 (s, 1H, $H^1$). FTIR (KBr), $\nu$ ($cm^{-1}$): 3261 (s, C≡CH), 3049 (m, Ar-H), 2956 (m, $-CH_3$), 2089 (w, C≡C), 1620, 884 (m, Ar).

**2.3.8. Preparation of ($W_{71}$).** To a 100 mL round bottom flask equipped with a magnetic stirring bar **6** (0.19 g 0.7 mmol), **Y** (0.03 g, 0.1 mmol), ODZMS (0.15 g, 0.1 mmol), KF (0.23 mg 4 mmol), and $Cu(PPh_3)_3Br$ (0.01 g, 0.08 mmol) in DMF (50 mL) were added, which was refluxed at 110 °C for 24 h. The reaction mixture was poured into a saturated solution of EDTA and the product was obtained by filtration. The crude product was purified by column chromatography on silica gel (eluent: dichloromethane)

to afford fuchsia crystal $\mathbf{W_{71}}$. The isolated yield of the product was 95%. $^1$H NMR (400 MHz, 298 K, $CDCl_3$): $\delta$ = 8.54 (s, 7H, H), 8.19 (s, 8H, H), 8.06 (m, 28H, H), 7.16–7.46 (m, 32H, H), 6.46 (s, 2H, H), 5.29 (s, 1H, H), 5.15 (S, 1H, H), 1.33 (m, 16H, H), 0.78–0.81 (m, 9H, H), 0.01–0.02 (m, 48H, H). $^{29}$Si NMR (400 MHz, solid, $\delta$): −65.3 (Ar–$CH_2$–Si), −79.8 (anthracene–$CH_2$–Si). FTIR (KBr), $\nu$ ($cm^{-1}$): 3054 (w, Ar-H), 2962, 2929, 2857 (m, –$CH_3$), 1630 (m, trizole), 1095 (s, Si–O–Si). MALDI-TOF MS $[C_{158}H_{152}N_{26}O_{21}Si_{16} + 2H]^+$: calcd $(M + 2H)^+/z$, 3196.7950; found $m/z$, 3196.7860. Anal. calcd for $C_{158}H_{152}N_{26}O_{21}Si_{16}$: C, 59.29; H, 4.79; N, 11.38. Found: C, 60.03; H, 4.737; N, 11.13.

**2.3.9. Preparation of ($\mathbf{W_{62}}$).** $\mathbf{W_{62}}$ was prepared using the above discussed procedure. The product was a yellow powder, yield 97%. $^1$H NMR (400 MHz, 298 K, $CDCl_3$): $\delta$ = 8.54 (s, 7H, H), 8.05–8.07 (m, 6H, H), 8.13–8.15 (s, 8H, H), 8.05–8.07 (m, 24H, H), 7.38–7.49 (m, 32H, H), 6.46 (s, 4H, H), 5.29 (S, 2H, H), 5.15 (S, 2H, H), 1.33 (m, 16H, H), 0.54–0.56 (m, 18H, H), 0.01–0.02 (m, 48H, H). $^{29}$Si NMR (400 MHz, solid, $\delta$): −64.8 (Ar–$CH_2$–Si), −79.1 (anthracene–$CH_2$–Si). FTIR (KBr), $\nu$ ($cm^{-1}$): 3053 (w; Ar-H), 2964, 2928, 2857 (m, –$CH_3$), 1650 (m, trizole), 1093 (s, Si–O–Si). MALDI-TOF MS $[C_{164}H_{160}N_{28}O_{22}Si_{16} + 2H]^+$: calcd $(M + 2H)^+/z$, 3320.8601; found $m/z$, 3320.8590. Anal. calcd for $C_{164}H_{160}N_{28}O_{22}Si_{16}$: C, 59.25; H, 4.85; N, 11.80. Found: C, 59.03; H, 4.658; N, 12.04.

**2.3.10. Preparation of ($\mathbf{W_{53}}$).** $\mathbf{W_{53}}$ was prepared using the above discussed procedure. The product was a purple powder, yield 92%.$^1$H NMR (400 MHz, 298 K, $CDCl_3$): $\delta$ = 8.54 (m, 5H, H), 8.12–8.19 (m, 8H, H), 8.06 (m, 20H, H), 7.44–7.58 (m, 32H, H), 6.46 (s, 6H, H), 5.29 (S, 3H, H), 5.15 (S, 3H, H), 1.33 (m, 16H, H), 0.78–0.83 (m, 27H, H), 0.01–0.02 (m, 48H, H). $^{29}$Si NMR (400 MHz, solid, $\delta$): −64.6 (Ar-$CH_2$–Si), −80.5 (anthracene-$CH_2$–Si). FTIR (KBr), $\nu$ ($cm^{-1}$): 3052 (w; ArH), 2963, 2927, 2859 (m, –$CH_3$), 1635 (m, trizole), 1099 (s, Si–O–Si). MALDI-TOF MS $[C_{170}H_{168}N_{30}O_{23}Si_{16} + H]^+$: calcd $(M + H)^+/z$, 3444.9257; found 3444.9190. Anal. calcd for $C_{170}H_{168}N_{30}O_{23}Si_{16}$: C, 59.21; H, 4.91; N, 12.18. Found: C, 58.73; H, 5.031; N, 11.97.

# 3. Results and discussion

## 3.1. Theoretical calculation

To validate the rationality of the structural design of chromophores, a theoretical calculation was conducted using the Gaussian09 software suite with a TD-DFT/6-31G+ level of theory, which was used to simulate the absorption and emission spectra of candidates **B** and **Y** in THF.[40,41] The calculation results are shown in Fig. 1. Here, chromophores **B** and **Y** with similar absorption spectra and a different Stokes shift in their emission spectra were selected. It can be concluded from Fig. 1 that **B** and **Y** show similar absorption spectra, so the same excited light source can be used. Meanwhile, the emission spectrum of **Y** displays a very large Stokes shift. This not only makes the emission spectra of **B** and **Y** cover the whole visible range of white light, but also inhibits the intramolecular self-absorption. Based on the highly efficient "click chemistry" and covalent incorporation of nano-sized inorganic POSSs, the novel hybrid white emission materials with high efficiency are successfully achieved by precisely adjusting the components of **B** and **Y**.

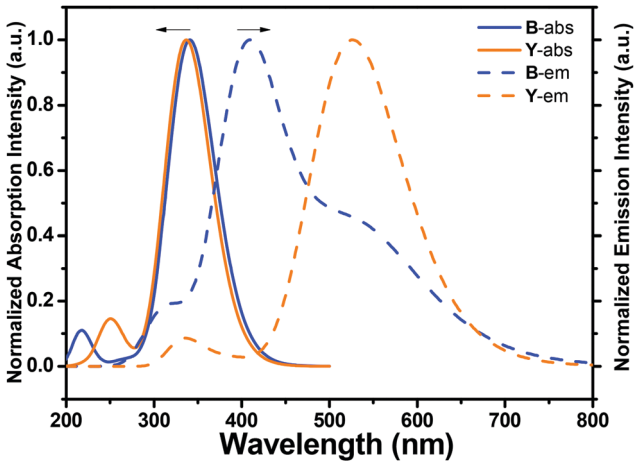


Fig. 1 The normalized calculated absorption and emission spectra of **B** and **Y** in THF.

## 3.2. Synthesis and characterization

Single molecule organic white light emitters (SMOLEDS) have exhibited some excellent advantages such as perfect color reproducibility, stability and easy fabrication. SMOLEDS mainly concentrated on a series of polymers. However, the inherent poor purity, multi-polydispersity and low thermal properties of polymers have greatly limited their luminous efficiency and practical applications. Hence, design and preparation of hybrid white-light-emitting macromolecules with high thermal properties and good luminous efficiency will be a key issue for their application in flexible displays. Based on the calculation of the density theory, three POSS-based luminous single molecular nanohybrids $\mathbf{W_{71}}$, $\mathbf{W_{62}}$ and $\mathbf{W_{53}}$ containing a yellow monochromatic emitter (**Y**) with a large Stokes shift and a blue monochromatic emitter (**B**), in which the front value in the subscript is defined as the number of **B** group, the latter value is the number of **Y** group, were designed and prepared.

**Y** and **B** were synthesized using Knoevenagel condensation and the Sonogashira reaction (ESI†). At first, 4-ethynylbenzaldehyde, a reactant of **Y**, was synthesized from 2-methyl-3-butyn-2-ol. However, intramolecular and intermolecular aldol condensation occurred during the hydrolysis reaction and the ideal compound was not obtained. Fortunately, after changing 2-methyl-3-butyn-2-ol to trimethylsilylacetylene, the problem was solved and 4-ethynylbenzaldehyde was prepared successfully. 2-(2-*tert*-Butyl-6-methylpyran-4-ylidene) malononitrile was prepared following the procedure reported in ref. 32. All the purified products exhibited characteristic FTIR and $^1$H NMR spectra(see the ESI† for details) and elemental analysis corresponding to their expected structures.

In the synthetic process of hybrids, a one-step synthesis strategy was employed using highly efficient click chemistry methods. The purification is easily achieved by simply dissolving the precipitates. Similar one-step strategies were reported in the literature.[33]

The structures of hybrids $\mathbf{W_{71}}$, $\mathbf{W_{62}}$ and $\mathbf{W_{53}}$ were determined by means of standard spectral methods, elemental analysis and mass spectra. Fig. 2a shows the FTIR spectra of $\mathbf{W_{71}}$, $\mathbf{W_{62}}$ and $\mathbf{W_{53}}$.

 

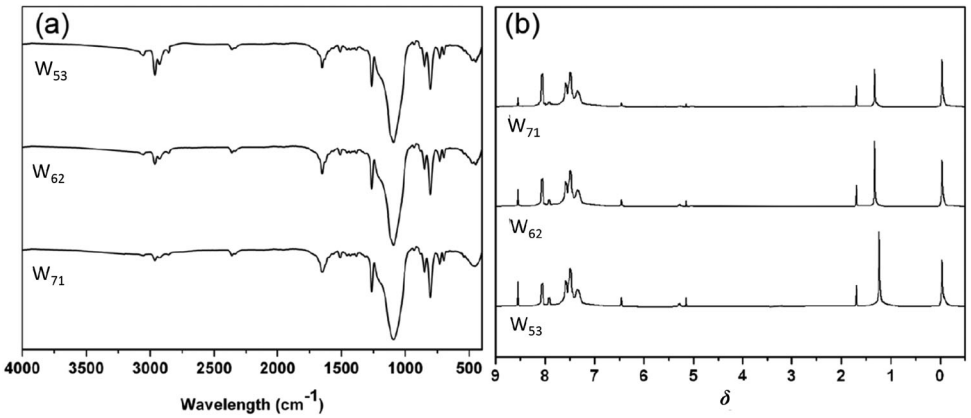


Fig. 2 The FTIR and $^1$H NMR spectra of $\mathbf{W_{71}}$, $\mathbf{W_{62}}$ and $\mathbf{W_{53}}$.

As shown in Fig. 2a, the characteristic absorptions at ~3100, 1625 $cm^{-1}$ corresponding to triazole stretching vibration absorption and the characteristic Si–O–Si stretching vibration of the POSS core at ~1100 $cm^{-1}$ appear in the spectra of the resulting hybrids, and the characteristic absorptions of $-N_3$ and C≡C at ~2100 $cm^{-1}$ disappear, indicating that all the eight azide groups of POSS-$N_3$ completely reacted with alkynyl groups of **B** and **Y** to form the resultant hybrids at almost stoichiometric pattern. In the $^1$H NMR spectra (Fig. 2b), it is also found that the characteristic alkyne proton absorption band located at 3.13 ppm in the spectra of **B** and **Y** completely disappears after click reactions and new vibration bands at 1.33 ppm (–SiC$H_2$) and 0.29 ppm (–SiC$H_3$) turn up in the $^1$H NMR spectrum of **ODZMS**, further supporting that objective molecules have been obtained. The characteristic spectral peaks at ~8.54 ppm, assigned to the H proton of triazole, were observed in the spectrum of the resultant hybrids, which further confirm that the click reactions were successfully performed. Moreover, the results of C, H, N elemental analyses almost completely correspond to the theoretically calculated values of the objective compounds, further supporting that the objective molecules were obtained.

### 3.3. Photophysical properties

All the resultant molecules $\mathbf{W_{71}}$, $\mathbf{W_{62}}$ and $\mathbf{W_{53}}$ are soluble in common organic solvents, such as dichloromethane (DCM), tetrahydrofuran (THF), dimethyl sulfoxide (DMSO), *etc.* The solution -based emission and absorption measurements were performed at very low concentrations ($10^{-5}$ M) in an intermediate dielectric constant solvent (THF, $\varepsilon$ = 7.6) to remove the effect of molecular aggregation and differences in molecular dipole moments.[53] The results shown that **Y**'s TLC plate showed a dark point at first, and then exhibited a yellow light point. This may be due to the restriction of intramolecular rotation (RIR) induced emission. Accordingly, the emission spectra of **Y** in a THF/water mixture solvent were tested (Fig. 3), where THF is a very good solvent and water is a poor solvent. It is found that, in good solvent THF, **Y** shows a weak emission at ~470 nm; but after the addition of poor solvent $H_2O$ (>40% v/v), **Y** exhibits a strong yellow light emission with

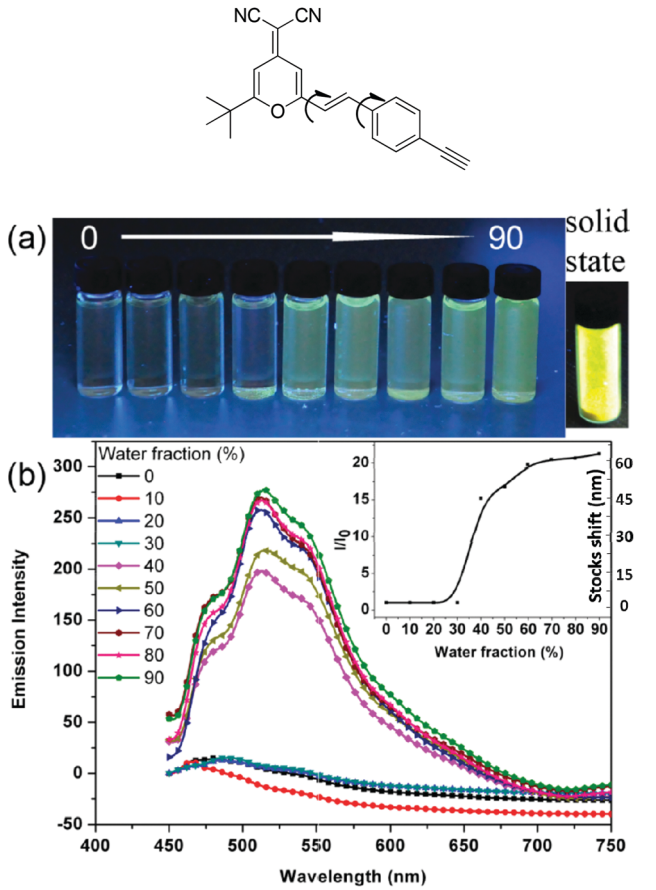


Fig. 3 The images of **Y** in the THF/water mixture solvent and the solid state (a) and emission spectra of **Y** in the THF/water mixture solvent (b) ($10^{-5}$ mol $L^{-1}$, $\lambda_{ex}$ = 365 nm). Inset: Changes in the PL peak intensities (*I*) and the Stokes shift (nm) of the corresponding molecules with different water fractions in the THF/$H_2O$ mixtures.

*ca.* 15 fold enhancement and two red shift enhanced emission peaks at ~530 nm and 570 nm.[28,35,53] Interestingly, at a low water content, the emission spectrum shows a significant blue shift, and then a red shift with an increase of the water content owing to the aggregation enhanced emission effect. Simultaneously, the emission intensity enhanced with an increase of the water

content (20 fold at 90 (v/v)% water content) while the **Y**'s Stokes shift did not change further after the water content became more than 40 (v/v)%. As shown in Fig. 3a, it emits a bright yellow light in the solid state under 365 nm UV light. These results further indicated that a yellow emitter with a large Stokes shift was obtained successfully. Moreover, different from **Y**, the emission spectra of **B** were quickly quenched after the poor solvent was added moreover, and generate strong fluorescence in the solid state. These shifts may be due to the dipole–dipole intramolecular interactions between organic moieties and POSS cages enlarging the torsion angle between the fluorine ring and the triazole ring and lowering the effective conjugation length of the molecules. Simultaneously, $\mathbf{W_{62}}$, $\mathbf{W_{53}}$, and $\mathbf{W_{71}}$ show a higher quantum yield of 95%, 83%, 81%, respectively, which are higher than 70% of **B** and 75% of **Y**.

To evaluate the rationality of our design strategy, the absorption and emission spectra of monochromatic emitters **B** and **Y** in THF and the THF/$H_2O$ mixture solvent were compared. Fig. 4 is the normalized absorption and emission spectra of **B** and **Y**. As shown in Fig. 4, **B** exhibits a strong absorption band from 315 to 475 nm, and **Y** shows a boarder absorption bond from 295 to 475 nm. They have an overlap between their absorption spectra at UV bands, which make sure that they can be excited at the same band light, such as 365 nm light from normal UV laps. Meanwhile, the absorption spectrum of **Y** and the emission spectrum of **B** weakly overlap between 390–475 nm, which effectively limit the intramolecular self-absorption of the resultant hybrids. In addition, the emission spectra of **B** and **Y** fully cover the light band from 400 to 700 nm, which makes the realization of white light emission possible.

To further investigate the intramolecular self-absorption of the resultant hybrids, the emission spectra of three hybrids in THF were measured. In a good solvent (THF), the emission of the **Y** unit is not strong enough to influence the emission spectrum of the **B** unit, and the change in the emission spectra of hybrids can be attributed to the intramolecular self-absorption from **B** to **Y**. As shown in Fig. 5, the emission spectrum of $\mathbf{W_{71}}$ shows three peaks at 385, 403 and 431 nm, respectively. With an increase in the ratio of the yellow unit in hybrids, the emission spectra of the resultant hybrids such as $\mathbf{W_{62}}$ and $\mathbf{W_{53}}$ exhibit two peaks at 410 and 440 nm, respectively. The short wave band UV emission peak at 385 nm disappeared due to intramolecular self-absorption, while the long blue wave band is well kept. These results reveal that the adjusted intramolecular self-absorption occurs in the resultant hybrids: on the one hand, the intramolecular self-absorption at the blue band was prohibited and the blue light-emitting component was well protected; on the

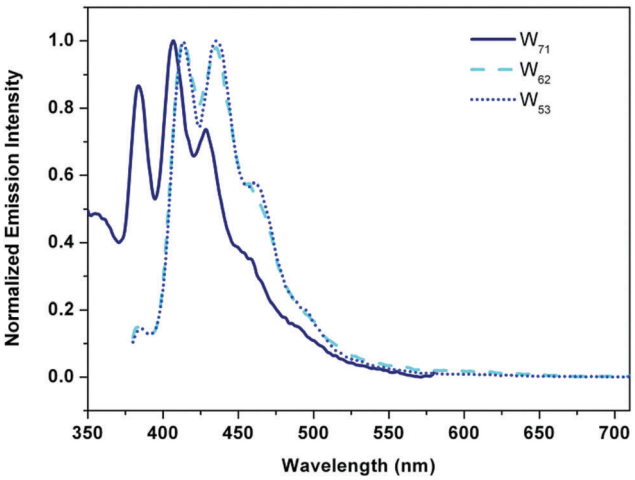


Fig. 5 The emission spectra of $\mathbf{W_{71}}$, $\mathbf{W_{62}}$ and $\mathbf{W_{53}}$ in THF ($10^{-5}$ mol $L^{-1}$, $\lambda_{ex}$ = 365 nm).

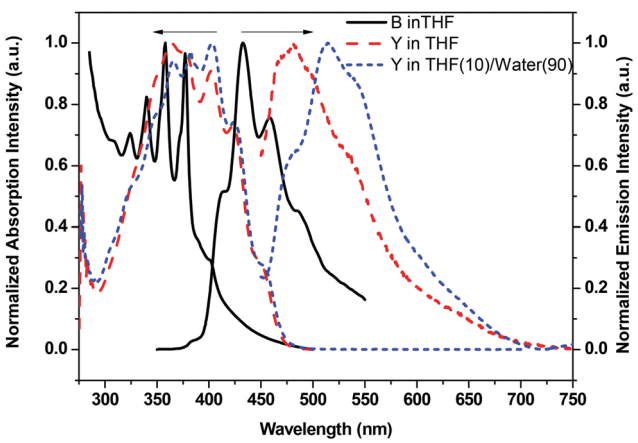


Fig. 4 The absorption and emission spectra of **B** and **Y** in THF and **Y** in THF/water (v/v = 10 : 90) mixture solvent ($10^{-5}$ mol $L^{-1}$, $\lambda_{ex}$ = 365 nm).

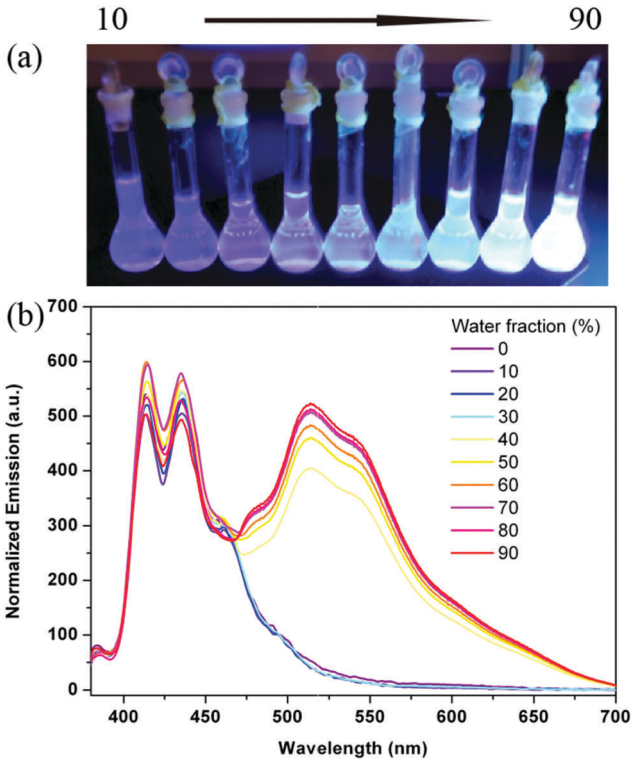


Fig. 6 The images (a) and emission spectra (b) of $\mathbf{W_{62}}$ in the THF/water mixture solvent ($10^{-5}$ mol $L^{-1}$, $\lambda_{ex}$ = 365 nm).

 

other hand, the UV-band emission of **B** was self-absorbed by **Y**, which enhances the yellow light-emitting component and further ensures equilibrious white light emission.

However, in a mixed solvent, these resultant hybrids show quite different spectral characteristics compared to their emission spectra in good solvent THF (Fig. 6). After the introduction of POSSs, the emission of hybrids with a blue band does not quench with the increase of the water content due to the disaggregation effect of the POSS cage. In contrast, the emission intensity shows a little increase, implying that the POSS cage does not prohibit the interactions between **Y** groups and solvent molecules, and the hybrids show an enhanced yellow band emission with the increase of the water content owing to the solvent effect. After adjustment of the ratio of **B** and **Y** in hybrids, $\mathbf{W_{71}}$ in the film shows light-blue emission due to the relatively weak yellow light, whereas $\mathbf{W_{53}}$ exhibits light-green emission due to the relatively strong yellow light (Fig. S22 and S23, ESI†). We successfully achieved white light emission from $\mathbf{W_{62}}$ (Fig. 6) in THF/water (10 : 90 v/v) and films (Fig. 7). And its Commission International d'Eclairage (CIE) coordinates is (0.29, 0.34) belonging to the white light range.

Fig. 7 shows the emission properties of $\mathbf{W_{62}}$ in the solid state. The film of $\mathbf{W_{62}}$ was prepared by spin-coating the hybrid solutions (*ca.* 10 mg $mL^{-1}$) on quartz plates at 1000 rpm for 30 s. To ensure the accuracy of measurement, three samples were all prepared under the same conditions. The AFM image of the $\mathbf{W_{62}}$ film show that its surface is quite smooth and no cracks and aggregation are observed (Fig. 7a), implying that the resultant organic hybrid has good film forming ability and structural homogeneity. And the emission spectrum of the $\mathbf{W_{62}}$ film is shown in Fig. 7c. As shown in Fig. 7c, the emission spectrum of the $\mathbf{W_{62}}$ film is similar to the emission spectrum of $\mathbf{W_{62}}$ in a poor solvent and exhibits a white-light emission over the whole visible range from 400 to 700 nm (Fig. 7b and c).

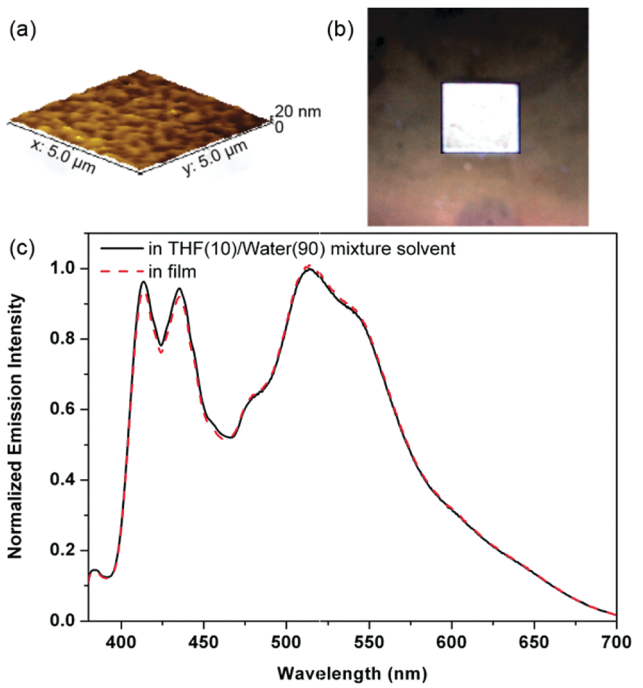


Fig. 7 (a) Atomic force microscope images of 5 × 5 $\mu m^2$ tapping mode of the $\mathbf{W_{62}}$ film; (b) the images of the $\mathbf{W_{62}}$ film under 365 nm UV; (c) the emission spectra of $\mathbf{W_{62}}$ in film and the THF/water (v/v = 10 : 90) mixture solvent ($\lambda_{ex}$ = 365 nm).

### 3.4. Thermal properties

The thermal properties of white light emitting hybrid $\mathbf{W_{62}}$ were measured using TGA and DSC (Fig. 8). Usually, the thermal decomposition behavior of POSS macromeres exhibits two step decompositions: the decomposition of the organic component and the inorganic POSS cage. However, the TGA curve of $\mathbf{W_{62}}$ only shows the one-step decomposition. Meanwhile, the $T_{d5\%}$ value of $\mathbf{W_{62}}$ is *ca.* 273 °C, which is much higher than 192 °C of **Y** and 205 °C of **B** (Fig. 8a). Moreover, the char yield of the thermally cured POSSAF was 37.4%, which is not only much higher than those of **B** and **Y** (almost no residual), but also higher than its theoretical residual rate (28.9%). The thermal stability enhancement and one-step decomposition behaviors are attributed to the uniform incorporation of the POSS cage and the jacket effect of the chromophore pendants:[35,44–48] that is, in which the POSS core may have been surrounded by a rigid jacket formed through the strong intra- and inter- molecular electronic interactions of the organic arms, shielding the molecules from thermal attack. Simultaneously, the triazole ring also enhances the thermal stability of the hybrid nanocomposite. Furthermore, as

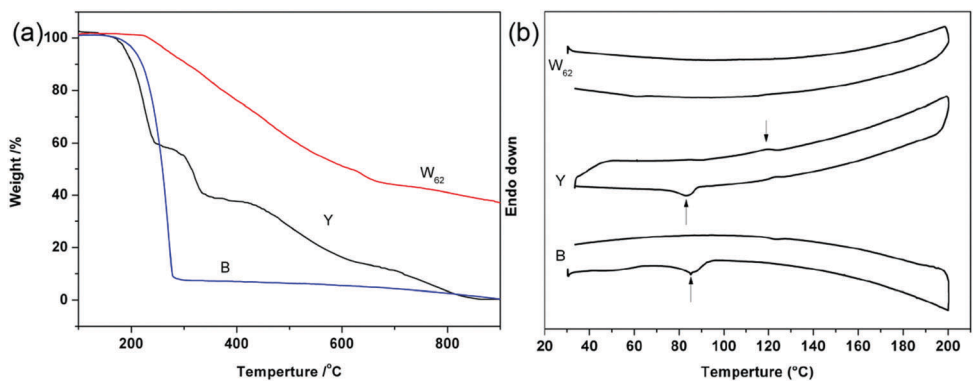


Fig. 8 The (a) TGA and (b) DSC curves of **B**, **Y** and $\mathbf{W_{62}}$.

the organic component is oxidized away from the surface, the remaining residue becomes enriched in silica and provides a barrier to further oxidation.[36,49–52] Especially, the DSC curves of **B** and **Y** both show a large melting point at ~85 °C, and **Y** exhibits a crystallization peak at ~120 °C. However, the DSC curve of $\mathbf{W_{62}}$ is quite smooth and there is no melting or crystallization point found (Fig. 8b). All these results reveal that the material $\mathbf{W_{62}}$ has an excellent amorphous state and high thermal stability.[53]

## 4. Conclusions

In conclusion, novel nano-sized hybrids with white light emission were realized by simple control of the feed ratio of blue and yellow monochromatic moieties in hybrids *via* highly efficient "click chemistry". Based on the theoretical simulations and molecular design, the optimized molecular structure and composition were obtained (component ratio of **B**:**Y** at 6:2). The investigation of the emission mechanism shows that the allowable transfer in the UV band improves the yellow light emission intensity and the restraint of energy transfer in the blue band ensures the blue light emission intensity and the balance of resultant white light emission based on a large Stokes shift of the yellow monochromatic emitter. The incorporation of nano-sized POSSs not only shows a significant AIE effect, but also exhibits high thermal stability, which efficiently enhance the efficiency ($\Phi_{film}$ = 95%) of the resultant hybrids ($\mathbf{W_{62}}$) in the solid state due to the deaggregation effect of POSS. This work provided a novel strategy for design and preparation of white-light-emitting molecules with high thermal stability, high emission efficiency and good film forming ability.

## Conflicts of interest

There are no conflicts to declare.

## Acknowledgements

This research was financially supported by the National Natural Science Fund of China (Grant No. 21671037, 21471030, 21277103, and 21271040).

## References

1 M. R. Molla and S. Ghosh, *Chem. – Eur. J.*, 2012, **18**, 1290–1294.
2 C. M. Zhong, C. H. Duan, F. Huang, H. B. Wu and Y. Cao, *Chem. Mater.*, 2011, **23**, 326–340.
3 Y. Zhang, C. A. Xie, H. P. Su, J. Liu, S. Pickering, Y. Q. Wang and J. A. Xu., *Nano Lett.*, 2011, **11**, 329–332.
4 L. X. Xiao, Z. J. Chen, B. Qu, J. X. Luo, S. Kong, Q. H. Gong and J. J. Kido, *Adv. Mater.*, 2011, **23**, 926–952.
5 S. Mukherjee and P. Thilagar, *Dyes Pigm.*, 2014, **110**, 2–27.
6 A. Ozawa, A. Shimizu, R. Nishiyabu and Y. Kubo, *Chem. Commun.*, 2015, **51**, 118–121.
7 C. Chen, X. H. Jin, X. J. Zhou, L. X. Cai, Y. J. Zhang and J. Zhang, *J. Mater. Chem. C*, 2015, **3**, 4563–4569.
8 B. J. Xu, Y. X. Mu, H. Z. Wu and Y. Zhang, *Chem. Sci.*, 2016, **7**, 2201–2206.
9 V. R. K. K. K. R. Datta and S. J. George., *Adv. Mater.*, 2013, **25**, 1713–1718.
10 P. Li, Q. Chen, J. Zhao, Z. Hu and D. Cao, *J. Surfactants Deterg.*, 2011, **15**, 449–456.
11 R. B. Wang, J. A. Peng, F. Qiu and Y. L. Yang, *Chem. Commun.*, 2009, 6723–6725.
12 H. Sasabe, J. Takamatsu, G. Wagenblast, N. Langer and J. Kido, *Adv. Mater.*, 2010, **22**, 5003–5007.
13 S. K. Panda, S. G. Hickey, H. V. Demir and A. Eychmuller, *Angew. Chem., Int. Ed.*, 2011, **50**, 4432–4436.
14 K. Kim, J. Y. Woo, S. Jeong and C. S. Han, *Adv. Mater.*, 2011, **23**, 911–914.
15 W. Mroz, C. Botta, U. Giovanella, E. Rossi and A. Colombo, *J. Mater. Chem.*, 2011, **21**, 8653–8661.
16 M. M. Zhang, S. C. Yin, J. Zhang and Z. X. Zhou, *Proc. Natl. Acad. Sci. U. S. A.*, 2017, **114**, 3044–3049.
17 D. Chen, J. Y. Zhan, M. M. Zhang and S. C. Yin, *Polym. Chem.*, 2015, **6**, 25–29.
18 J. Liu, Y. Cheng, Z. Xie, Y. Geng, L. Wang, X. Jing and F. Wang, *Adv. Mater.*, 2008, **20**, 1357–1362.
19 J. Liu, L. Chen, S. Shao, Z. Xie, Y. Cheng, Y. Geng and F. Wang, *Adv. Mater.*, 2007, **19**, 1859–1863.
20 H. Wu., J. Zou, F. Liu, L. Wang and A. Mikhailovsky, *Adv. Mater.*, 2008, **20**, 696–702.
21 L. Ying, C. Ho and H. Wu, *Adv. Mater.*, 2014, **16**, 2459–2473.
22 C. Gu, Y. Chen and Z. Zhang, *Adv. Energy Mater.*, 2014, **8**, 1289–1295.
23 S. Park, J. E. Kwon, S. H. Kim, J. Seo and K. Chung, *J. Am. Chem. Soc.*, 2009, **131**, 14043–14049.
24 S. H. Kim, S. Park, J. E. Kwon and S. Y. Park, *Adv. Funct. Mater.*, 2011, **21**, 644–651.
25 X. H. Yang, J. D. Froehlich, H. S. Chae and S. Li, *Adv. Funct. Mater.*, 2009, **19**, 2623–2629.
26 K. Tanaka and Y. Chujo, *J. Mater. Chem.*, 2012, **22**, 1733–1746.
27 F. Wang, X. Lu and C. He, *J. Mater. Chem.*, 2011, **21**, 2775–2782.
28 Z. Yan, H. Xu, S. Guang, X. Zhao, W. Fan and X. Y. Liu, *Adv. Funct. Mater.*, 2012, **22**, 345–352.
29 B. H. Yang, H. Y. Xu, Z. Z. Yang and C. Zhang, *J. Mater. Chem.*, 2010, **20**, 2469–2473.
30 X. Y. Su, S. Y. Guang, C. W. Li and H. Y. Xu, *Macromolecules*, 2010, **43**, 2840–2845.
31 B. H. Yang, H. Y. Xu, Z. Z. Yang and X. Y. Liu, *J. Mater. Chem.*, 2009, **19**, 9038–9044.
32 C. Zhang, S. Guang, X. Zhu, H. Xu, X. Liu and M. Jiang., *J. Phys. Chem. C*, 2010, **114**, 22455–22461.
33 X. Y. Su, S. Y. Guang, H. Y. Xu, X. Y. Liu, S. Li, X. Wang and P. Wang, *Macromolecules*, 2009, **42**, 8969–8976.
34 (*a*) Y. Feng, Y. Jia and H. Y. Xu, *J. Appl. Polym. Sci.*, 2009, **111**, 2684–2690; (*b*) Y. D. Xu, Q. Yang, Z. H. Shen, X. F. Chen, X. H. Fan and Q. F. Zhou, *Macromolecules*, 2009, **42**, 2542–2550.
35 Y. K. Zhu, S. Y. Guang and H. Y. Xu, *Chin. Chem. Lett.*, 2012, 1095–1098.
36 S. Sulaiman, A. Bhaskar, J. Zhang and R. Guda, *Chem. Mater.*, 2008, **20**, 5563–5573.

 

37 T. Stephan and K. Norbert., *J. Org. Chem.*, 1998, **63**, 8551–8553.
38 J. Wilbuer, D. C. Grenz, G. Schnakenburgc and B. Esser, *Org. Chem. Front.*, 2017, **4**, 658–663.
39 K. C. Tanja, T. Siham, W. Alexander and B. Martin, *Chem. Commun.*, 2017, **53**, 1599–1602.
40 Z. Z. Li, F. Liang, M. P. Zhuo, Y. L. Shi and X. D. Wang, *Small*, 2017, **13**, 1604110.
41 Z. Wang, B. Lin, X. Hu and C. Zhang, *ACS Appl. Mater. Interfaces*, 2017, **9**, 35253–35259.
42 B. Minaev, G. Baryshnikov and H. Agren, *Phys. Chem. Chem. Phys.*, 2014, **16**, 1719–1758.
43 U. Giovanella, C. Botta, F. Galeotti, B. Vercelli, S. Battiato and M. Pasini, *J. Mater. Chem. C*, 2013, **1**, 5322–5329.
44 Y. K. Zhu, S. Y. Guang, H. Y. Xu, X. Y. Su and X. Y. Liu, *J. Mater. Res.*, 2013, **8**, 1061–1069.
45 Y. K. Zhu, S. Y. Guang, X. Y. Su, H. Y. Xu and D. Y. Xu, *Dyes Pigm.*, 2013, **97**, 175–183.
46 X. Y. Su, S. Y. Guang, H. Y. Xu, J. Y. Yang and Y. L. Song., *Dyes Pigm.*, 2010, **87**, 69–75.
47 F. Y. Ke, C. Zhang, S. Y. Guang, H. Y. Xu and N. B. Lin, *J. Appl. Polym. Sci.*, 2015, **132**, 42292.
48 X. Wang, S. Y. Guang, H. Y. Xu, X. Y. Su and N. B. Lin, *J. Mater. Chem.*, 2011, **21**, 12941–12948.
49 S. Z. Wang, S. Y. Guang, H. Y. Xu and F. Y. Ke, *RSC Adv.*, 2015, **5**, 1070–1078.
50 F. Y. Ke, S. Z. Wang, S. Y. Guang, Q. Liu and H. Y. Xu, *Dyes Pigm.*, 2015, **121**, 199–203.
51 X. Wang, S. Y. Guang, H. Y. Xu, X. Y. Su, J. Y. Yang, Y. L. Song and N. B. Lin, *J. Mater. Chem.*, 2008, **18**, 4204–4209.
52 C. Zhang, S. Y. Guang, X. B. Zhu, H. Y. Xu, X. Y. Liu and M. H. Jiang, *J. Phys. Chem. C*, 2010, **114**, 22455–22461.
53 Y. K. Zhu, S. Y. Guang, H. Y. Xu, X. Y. Su and X. Y. Liu, *J. Mater. Chem. C*, 2013, **1**, 5277–5284.